Influence of incidence angle in the correlation of C-band polarimetric parameters with biophysical variables of rainfed crops

Rubén Valcarce-Diñeiro[a]*, Juan M. Lopez-Sanchez[b], Nilda Sánchez[a,c], Benjamín Arias-Pérez[a], José Martínez-Fernández[c]

[a]*Department of Cartographic and Land Engineering, University of Salamanca, Hornos Caleros 50, 05003 Ávila, Spain*

[b]*IUII, University of Alicante, P.O. Box 99, E-03080, Alicante, Spain*

[c]*CIALE, University of Salamanca, Duero 12, 37185 Villamayor, Salamanca, Spain*

*corresponding author: Rubén Valcarce-Diñeiro, ruben.v.d@usal.es, Department of Cartographic and Land Engineering, University of Salamanca, Hornos Caleros 50, 05003 Ávila, Spain

Influence of incidence angle in the correlation of C-band polarimetric parameters with biophysical variables of rainfed crops

ABSTRACT: A multi-temporal field experiment was conducted within the Soil Measurement Stations Network of the University of Salamanca (REMEDHUS) in Spain in order to retrieve useful crop information. The objective of this research was to evaluate the potential of polarimetric observations for crop monitoring by exploiting a time series of 20 quad-pol RADARSAT-2 images at different incidence angles (i.e., 25º, 31º and 36º) during an entire growing season of rainfed crops, from February to July 2015. The time evolution of six crop biophysical variables was gathered from the field measurements, whereas ten polarimetric parameters were derived from the images. Thus, a subsequent correlation analysis between both datasets was performed. The study demonstrates that the backscattering ratios (HH/VV and HV/VV), the normalized correlation between HH and VV (γ_{HHVV}), and the dominant alpha angle (α_1), showed significant and relevant correlations with several biophysical variables such as biomass, height, or leaf area index (LAI) at incidence angles of 31º or 36º. The joint use of data acquired with different beams could be exploited effectively to increase the refresh rate of information about crop condition with respect to a single incidence acquisition scheme.

RÉSUMÉ: Sur le site du Réseau des Stations de Mesure des Sols de l'Université de Salamanca (REMEDHUS) en Espagne, un suivi multitemporelle de diverses cultures a été réalisée de radar à ouverture. L'objectif de cette recherche est d'analyser le potentiel des observations polarimétriques pour la surveillance de cultures exploitant une série temporelle d'images quad-pol RADARSAT-2 sous différents angles d'incidence (c'est-à-dire 25º, 31º et 36º) durant toute la période de croissance. Vingt images de RADARSAT-2 ont été obtenues dans la zone d'étude entre les mois de février et juillet 2015. Six variables biophysiques ont été mesurées sur le terrain et dix paramètres polarimétriques ont été dérivés des images. Une analyse de corrélation a été réalisée entre les ensembles de données. L'étude montre que les relations de rétrodispersion (HH/VV et HV/VV), la corrélation normalisée entre HH et VV (γ_{HHVV}) et l'angle alpha dominant (α_1) présentent des corrélations significatives et importantes avec divers variables biophysiques comme la biomasse, la hauteur ou l'indice de surface foliaire (LAI) pour des angles d'incidence de 31º à 36º. On pourrait profiter de l'utilisation

conjointe de ces deux angles pour augmenter le taux d'information sur l'état des cultures par rapport à un seul schéma d'acquisition d'incidence.

Keywords: biophysical variables, C-band, incidence angle, polarimetric SAR, RADARSAT-2

Introduction

Synthetic Aperture Radar (SAR) satellite data are useful for mapping and monitoring agriculture because microwave frequencies operate night and day in all weather conditions, and agricultural targets such as soils and crops are very dynamic. Contrarily, optical sensors can miss crucial periods during the growing season due to the presence of clouds. The potential of SAR data is based on the sensitivity of the radar backscattering to the dielectric properties and structure of the targets (i.e., the size, shape and orientation of the distribution of the elements in the scene) (Ulaby et al. 1984; Skriver et al. 1999; McNairn and Brisco 2004).

Crop monitoring approaches that employed early SAR instruments exploited only the backscattering coefficient, usually on a single polarization channel, which was the only observation provided from the operational sensors at that time. Unfortunately, different site properties (e.g., soil roughness and moisture, and vegetation properties) lead to similar values and equivalent changes in the backscattering coefficient, so crop monitoring with SAR was not very successful (Steele-Dunne et al. 2017). This situation started to change in 2007 with the launch of ALOS-PALSAR by the Japan Aerospace Exploration Agency (JAXA), RADARSAT-2 by the Canadian Space Agency (CSA) and TerraSAR-X by the German Aerospace Centre (DLR), for which polarimetric information (i.e., correlations and phase difference between channels) is also available. The new coherent polarimetric acquisitions opened new perspectives for the features to be studied when trying to build a crop monitoring application. In the future, the

RADARSAT Constellation Mission (RCM) (Thompson 2015) will continue providing the necessary polarimetric information for agriculture monitoring.

In order to design a crop monitoring application that uses SAR images, it is necessary to analyse the sensitivity of the radar parameters (i.e., the backscattering coefficient or any other variable derived from the radar measurements) with respect to the biophysical variables that describe the crop conditions on each acquisition date. Some examples in the literature show a correlation of crop parameters with polarimetric radar parameters, both for specific crops such as rice (Inoue et al. 2002, 2014; Inoue and Sakaiya 2013), maize (Bériaux et al. 2015), or several crop types simultaneously (Ulaby et al. 1984; Cable et al. 2014; Wiseman et al. 2014).

From pioneering studies (Ulaby et al. 1984) to more recent studies (Inoue et al. 2002), ground-based scatterometers at different frequencies, polarizations and incidence angles have shown sensitivity and good correlations to crop parameters. The use of RADARSAT-2 as a satellite sensor with polarimetric capabilities for crop monitoring was initiated with field campaigns in Canada in 2008, and also explored by the ESA-funded AgriSAR2009 campaign. One of the first full papers exploiting these data was published by Moran et al. (2012), in which the backscattering coefficients for all polarization channels were obtained from a time series of 57 RADARSAT-2 quad-polarization images acquired at C-band at different incidence angles from April to September 2009 for fields of wheat, barley, oat, corn, onion, and alfalfa. The cross-polarized channel was useful for monitoring both crop and soil conditions and was shown to be least sensitive to differences in the incidence angle. The time series offered reliable information about crop phenology. A positive correlation was found between the backscattering coefficients and the normalized difference vegetation index (NDVI) for onion and corn but not for all crops, and the impact of the view direction and the

incidence angle on the time series was minimal compared to the signal response of crop and soil conditions. Inoue and Sakaiya (2013) and Inoue et al. (2014) studied the correlation of the backscattering coefficients obtained at X-band (COSMO SkyMed) and C-band (RADARSAT-2) for rice canopies, suggesting the potential of satellite SAR images for the direct assessment of rice yield and other parameters (leaf area index (LAI), leaf biomass, and fraction of absorbed photosynthetically active radiation (fAPAR)) at a regional scale. More recently, Bériaux et al. (2015) studied C-band quad polarimetric satellite data for retrieving LAI and soil moisture in maize fields. The cross-polarization sensitivity was highlighted, especially for a high LAI, and the VV (vertical transmit and receive) polarization was found to be sensitive for LAI values less than 2.

All these studies aforementioned used only backscattering coefficients in one or more polarimetric channels, so no other polarimetric observations were analyzed. Other studies have enlarged the set of parameters beyond the backscattering coefficients. Cable et al. (2014), using RADARSAT-2 images at two incidence angles, analyzed how changes in the acquisition time and the incidence angle affected C-band polarimetric parameters for various crops such as barley, canola, oat, soybean, and wheat. The backscattering coefficients for all targets were higher when acquired at a steeper incidence angle (26º). All cash crop targets showed a rise and fall in the backscattering response during the course of the growing season, coinciding with the changing growth stages. Jiao et al. (2011) evaluated 18 polarimetric parameters derived from quad-pol RADARSAT-2 images at steep (25º) and shallow (40º) incidence angles with LAI of corn and soybean. They found that corn and soybean LAI was better correlated with polarimetric parameters sensitive to volume scattering (HV, LL, RR, pedestal height

and volume scattering from Freeman-Durden decomposition) with the steeper incidence angle.

The polarimetric response plots and decompositions offered insight into the scattering mechanism for each crop type and generally showed an increase in volume scattering as the crops reach maturity. Specifically, the primary scattering type shifted from surface scattering to volume scattering as the crops matured, both in regards to the Cloude and Pottier (1997) and Freeman and Durden (1998) decompositions. Wiseman et al. (2014) compared 21 polarimetric parameters derived with RADARSAT-2 images with dry biomass of canola, corn, soybean, and spring wheat. During the period of biomass accumulation, significant correlations with dry biomass were observed for most SAR parameters in corn, canola, and soybeans, which could prove to be useful as indicator of harvest timing. Adams et al. (2013b) investigated the Cloude-Pottier and Freeman-Durden scattering decompositions of RADARSAT-2 C-band data to identify harvested fields. The research reported that polarimetric scattering decomposition applied to shallower incidence angle acquisitions may provide utility for agricultural monitoring due to the characterization of unique scattering mechanism from soils and biomass. Other studies that use a varied set of polarimetric parameters can be found in Lopez-Sanchez et al. (2012, 2014). These parameters, computed at X-band with dual-pol data from TerraSAR-X and at C-band with quad-pol data from RADARSAT-2, respectively, were used to track phenological changes in rice fields. Adams et al. (2013a) employed a set of polarimetric parameters from RADARSAT-2 data at different incidence angles to assess the sensitivity of these parameters to unvegetated agricultural surface features. Smith and Buckley (2011) derived the three Freeman-Durden decomposition parameters from RADARSAT-2 images to monitor grasslands and generate land cover maps.

The overall goal of this research is to extend the knowledge about the potential of polarimetric parameters (i.e., beyond the backscattering coefficients) for crop monitoring. This objective is more ambitious than in previous studies because three overlapped time series of quad-pol RADARSAT-2 images were acquired at three different incidence angles. The field campaign took place in seven plots of rainfed crops during their growing season in central Spain in 2015. The resulting data set of plant and canopy parameters was compared with the polarimetric parameters derived from the RADARSAT-2 images by applying a correlation analysis.

The novel contribution of this study is the investigation of the effect of incidence angle on the correlation between polarimetric parameters and biophysical variables. This effect was studied in the past mostly with ground-based systems (Della Vecchia et al. 2006), but only a few examples with satellite data exist in the literature (Cable et al. 2014; Lopez-Sanchez et al. 2015). Hence, this study could help enlighten the choice of the best incidence angle for crop monitoring, as well as determining which parameters are less affected by changes in the incidence angle (hence enabling the combination of different beams for decreasing the time interval between images, which is key for monitoring applications).

Materials and methods

Study area and field campaign

The field campaign took place in 2015 during the rainfed crop growing season in an agricultural area in the central part of the Duero Basin in Spain (Figure 1). In this area, the Soil Moisture Stations Network of the University of Salamanca, REMEDHUS (Sánchez et al. 2012a), is routinely providing soil moisture and other agro-climatic data, which have been used in remote sensing and modelling applications. For this reason,

REMEDHUS is a validation core site of several microwave passive sensors (González-Zamora et al. 2016; Colliander et al. 2017). Additionally, data from active sensors were also tested in REMEDHUS, as the scatterometer onboard the European Remote Sensing Satellites (ERS) and its successor, the Advanced Scatterometer (ASCAT) (Ceballos et al. 2005; Brocca et al. 2011). REMEDHUS comprises a set of soil moisture and weather stations that provide a continuous time series from 1999 until the present. The area is mainly agricultural and has a continental semi-arid Mediterranean climate. The rainfed crops are the most common land cover in the area, comprising approximately 80% of the entire site (Sánchez et al. 2010), and are mainly winter cereals, seeded in October and harvested at the end of June or the beginning of July. The field measurements for this experiment were made in the plots corresponding to seven REMEDHUS stations, namely J12, K10 and L7 (wheat), F11 and M9 (barley), N9 (rye) and H9 (natural pasture). The pasture plot (H9) is a natural area without any agricultural nor livestock use, but a random mix of different grasses. The measurements were acquired throughout the growing season, i.e., from February to July 2015, every fortnight (n=9), one sample per plot over a frame of 1 m^2.

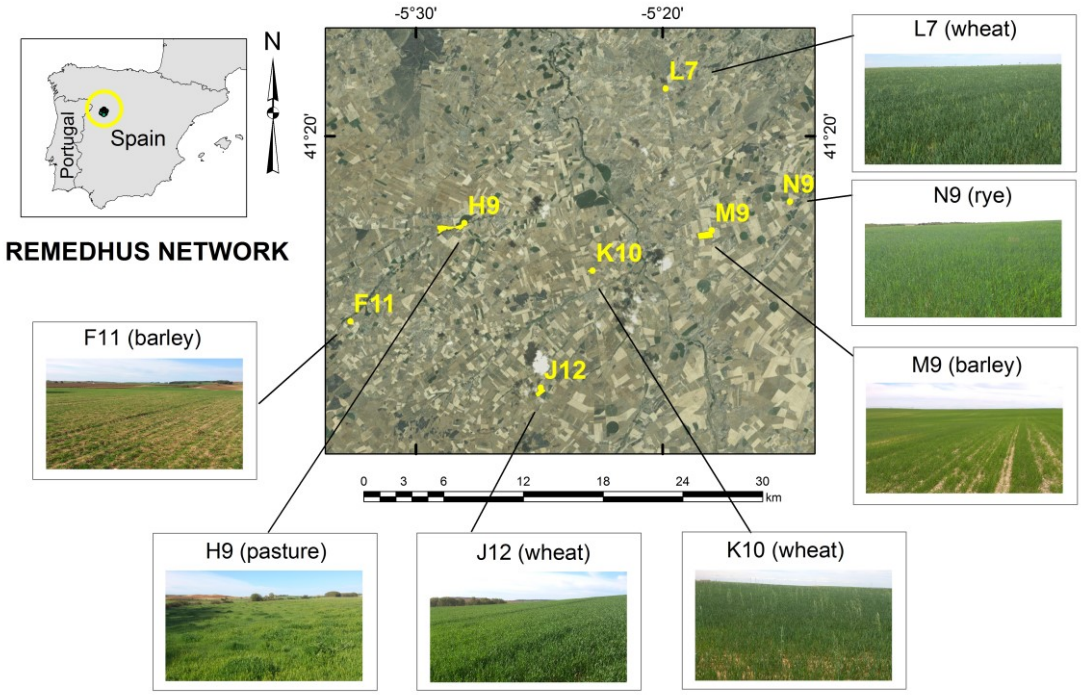

Figure 1. Study area, location of field plots and a general view of the different vegetation types.

In each plot, canopy height was directly measured and zenithal photographs were taken before the sampling. The phenological stages of the cereals were registered using a scale with 5 main intervals: 1) early vegetative phase (DoY=0-70), 2) plant emergence (DoY=71-100), 3) advanced vegetative phase (DoY=101-115), 4) reproductive phase (DoY=116-135), and 5) maturation phase (DoY=136-end).

Later on in the laboratory, LAI, the fraction of vegetation cover (FVC), the fresh and dry weights, the vegetation water content (VWC) and the percentage of water content (PWC) were estimated. These parameters have been used frequently in the related literature (Jackson et al. 2004; Jiang et al. 2006). The measurement protocols followed those described in Sánchez et al. (2012b). The green LAI was estimated via a destructive method in which photosynthetically active leaves were extracted from the sample, and then scanned and scaled to retrieve the areal value. Then, the sample was

dried until reaching a constant weight in an oven at 70°C for at least 24 h. The VWC was estimated as the difference between the wet and dry weights, considering the total amount of water in the stems and leaves. PWC is the ratio (in %) between the VWC and the fresh weight. Finally, the FVC was estimated from the digital photographs using a supervised classification. Soil moisture (SM) measurements from the REMEDHUS stations were also collected, coinciding with the date and time of the measurements. Hydra Probes Soil Sensors (Stevens® Water Monitoring System Inc.) are installed at a depth of 5 cm in each plot for this purpose.

SAR data and pre-processing

Polarimetric C-band (5.405 GHz) RADARSAT-2 imagery was used in this study. RADARSAT-2 has a repeat orbit of 24 days, but its different beam modes enable more frequent revisiting. Three sets of Fine Quad-Pol RADARSAT-2 Single Look Complex (SLC) images were acquired with average incidence angles of 25°, 31° and 36° (Table 1). Twenty images were acquired over the study area between February and July 2015. These images can be grouped in three series, comprising 7 images at 36°, 7 at 31°, and 6 at 25° (Table 1).

Table 1. List of available RADARSAT-2 images and their correspondence with field measurements

Acquisition Date	Day of Year (DoY)	Beam Mode	Average Incidence Angle (º)	Field Measurements
16-February-2015	47	FQ16W	36	17-February-2015 03-March-2015
23-February-2015	54	FQ11W	31	
12-March-2015	71	FQ16W	36	
19-March-2015	78	FQ11W	31	19-March-2015
26-March-2015	85	FQ6W	25	
05-April-2015	95	FQ16W	36	08-April-2015

12-April-2015	102	FQ11W	31	
19-April-2015	109	FQ6W	25	21-April-2015
29-April-2015	119	FQ16W	36	
06-May-2015	126	FQ11W	31	06-May-2015
13-May-2015	133	FQ6W	25	19-May-2015
23-May-2015	143	FQ16W	36	
30-May-2015	150	FQ11W	31	02-June-2015
06-June-2015	157	FQ6W	25	
16-June-2015	167	FQ16W	36	16-June-2015
23-June-2015	174	FQ11W	31	
30-June-2015	181	FQ6W	25	
10-July-2015	191	FQ16W	36	
17-July-2015	198	FQ11W	31	
24-July-2015	205	FQ6W	25	

Image processing was performed with the freely accessible Sentinel-1 Toolbox SNAP (Sentinel Application Platform) provided by the European Space Agency (ESA). The RADARSAT-2 images are provided with a polarimetric calibration already applied, so just the corresponding look-up-table was employed to convert them radiometrically to represent the backscattering coefficients. Then, the polarimetric coherency matrix (Cloude and Pottier 1996) was generated for each pixel in an image. A 9x9 boxcar filter was applied to reduce the speckle noise. With reference to the specification of these RADARSAT-2 images, the equivalent number of looks provided by such 9x9 filtering is above 48, which is large enough to obtain a reliable estimate of all polarimetric parameters in the subsequent analysis. For the parameters derived from the Eigen-decomposition of the coherency matrix, it is known that the necessary number of looks may be larger than 48 (Lee et al. 2008), but no significant differences were detected when the window size was increased above 9x9. Therefore, the same window size was used for all parameters. The Range Doppler orthorectification method available in

SNAP was applied for terrain correction and geocoding, using the digital elevation model from the Shuttle Radar Topography Mission. The final spacing of the geocoded images was 5 m. Geocoding was applied to all the entries of the filtered coherency matrices, i.e., a polarimetric coherency matrix was obtained at each geocoded pixel. Before the SAR parameters were estimated at field level, a 5-pixel erosion was carried out for all fields to prevent adjacent plot pixels from affecting the results.

Polarimetric SAR parameters

Seven polarimetric parameters (Table 2) were computed from the coherency matrices available for each pixel after geocoding. All parameters were obtained using the free-access PolSARpro software provided by ESA. The symbol used hereafter to denote them is shown in Table 2.

Table 2. List of polarimetric parameters analyzed in this study

Polarimetric parameter	Symbol
Backscattering coefficient at HH, HV and VV channels	σ^0_{HH}, σ^0_{HV}, σ^0_{VV}, or simply HH, HV and VV
Ratio of backscattering coefficients at HH, HV and VV channels	HH/VV, HV/VV
Normalized correlation (coherence) between the copolar channels (HH and VV)	γ_{HHVV}
Dominant alpha angle (from the Eigen decomposition of the coherency matrix)	α_1

The first group of selected parameters correspond to those which can be obtained directly from the polarimetric covariance matrix C, which is derived from the data gathered in the linear basis (horizontal and vertical polarizations) and arranged using the lexicographic basis (Cloude and Pottier 1996). These parameters are the backscattering coefficients and ratios, obtained from the diagonal of the covariance matrix C, and the correlations between channels (i.e., the amplitudes and phases)

obtained from the rest of the entries of the matrix C. The mathematical expression of these parameters is as follows (see Table 2 for notation):

$$\sigma_{HH}^{0} = 10\log_{10}\big(C(1,1)\big) \quad (1)$$

$$\sigma_{HV}^{0} = 10\log_{10}\big(C(2,2)\big) \quad (2)$$

$$\sigma_{VV}^{0} = 10\log_{10}\big(C(3,3)\big) \quad (3)$$

$$HH/VV = 10\log_{10}(C(1,1)/C(3,3)) \quad (4)$$

$$HV/VV = 10\log_{10}(C(2,2)/C(3,3)) \quad (5)$$

$$\gamma_{HHVV} = |C(1,3)|/sqrt(|C(1,1)| * |C(3,3)|) \quad (6)$$

The dominant alpha angle (α_1) was also tested because it is widely used in the literature on SAR polarimetry and provides a clear physical interpretation of the data. It is important to note that the correlations between the cross-polar channel and the co-polar channels, i.e., γ_{HHHV} and γ_{HVVV}, are not considered in the study because for natural surfaces they are very small due to reflection symmetry (Cloude and Pottier 1996). Additional parameters, such as the backscattering level in the Pauli basis or the outputs of model-based decompositions (Freeman and Durden 1998), are not included in the present study to limit its length and the final number of results. In the same vein, additional analyses could be done by exploiting other variations in the polarimetric basis (e.g., circular polarizations) or by selecting specific measurement modes (e.g., compact polarimetry). All these options are meant to be the objective of further research.

Correlation between SAR parameters and biophysical variables

A correlation analysis was carried out between all SAR parameters acquired at different incidence angles (25°, 31° and 36°), and the monitored biophysical variables. MATLAB was employed to apply a spline interpolation of the ground measurements in order to match the dates of RADARSAT-2 images (Table 1). Regarding the spatial matching, a cubic interpolation of the values at each neighboring grid point was applied. The correlation coefficient (Pearson's r) between each parameter and the 6 biophysical variables is computed, separately for all the 7 crop fields and the 3 different incidence angles. The number of samples used to calculate r was 9, corresponding to the number of the field measurements along the growing cycle. The statistical significance was evaluated at a 95% confidence level (p-value=0.05). For a better understanding of the correlations results, different thresholds were established to classify r: moderate (+/-0.66 to 0.75), high (+/-0.75 to 0.85) and very high (+/-0.85 to 1).

Results and discussion

Behavior of biophysical variables

The temporal evolution of each parameter for each crop type was derived from the *in situ* measurements (Figure 2). Crop height (Figure 2) showed a similar growth pattern for wheat, pasture and barley (except for F11, with some delay), with maxima at the beginning of the maturity phase (DoY=126), which remained until senescence. The data clearly show that rye (N9) is much taller than the other land cover types evaluated.

The highest density for the FVC (Figure 2) was found for pasture (H9), which had higher values during winter, since natural pasture has an annual cycle. In contrast, cereals showed an increasing trend at the beginning of the campaign, reaching a maximum of FVC approximately at the maturation phase (DoY=126), then a plateau-shaped behavior for rye and wheat, and a peak for barley. It is important to clarify that

the FVC parameter considers only green cover. At the last dates (DoY=160), the crops are still standing but the plants are totally dry (in senescence stage), thus FVC=0 despite vegetation heights are large. The LAI evolution (Figure 2) showed the highest values for pasture, in accordance with the FVC, owing to its dense coverage. Barley showed the smallest LAI and a slight delay in comparison to wheat and rye, which started earlier (especially rye). All the biomass curves (Figure 2) have a similar pattern. The highest biomass ranged from 1 kg m^{-2} to 2 kg m^{-2} and corresponded to the pasture area, followed by wheat, rye and barley. This biomass behavior represents the typical crop growth curve and is similar to the LAI behavior. The PWC (Figure 2) is very different from the rest of the vegetation parameters; a descending general trend is observed, although with some fluctuation. The consumption of water decreases towards the end as the plants dry out. This trend is confirmed by the soil moisture behavior (Figure 2), since the soil water content decreased throughout the growing cycle, even if small rainfall events occurred. These results were generally similar to those obtained in a previous field study in REMEDHUS for barley and pasture crops, described in Sánchez et al. (2012b).

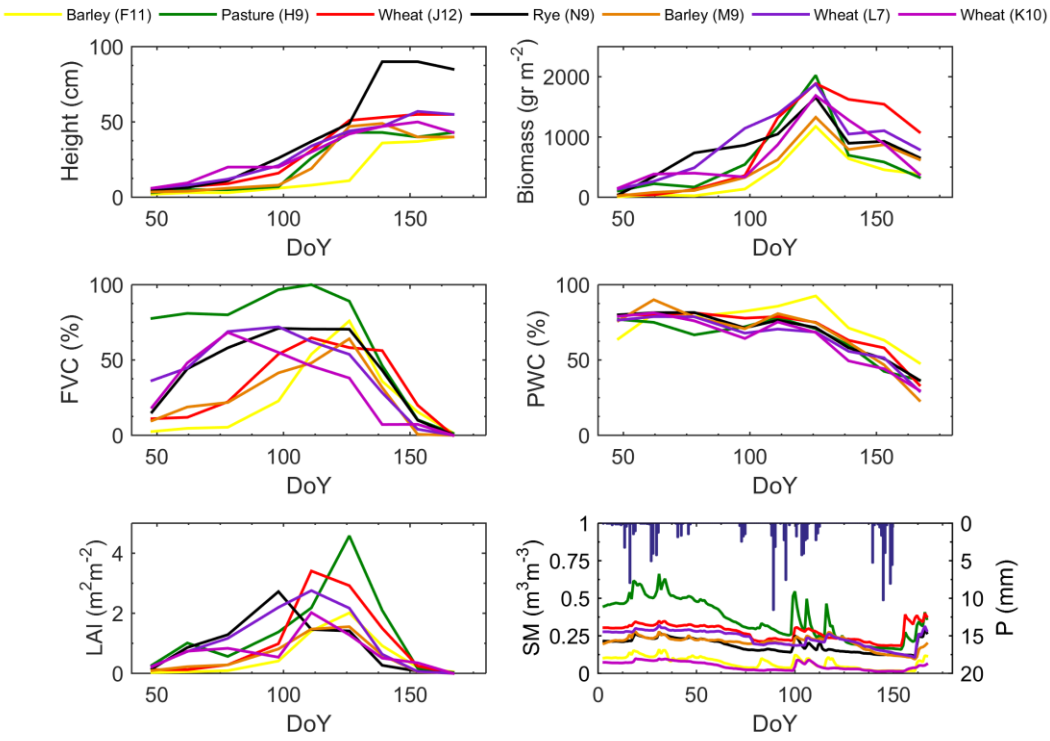

Figure 2. Evolution of height, FVC, LAI, biomass, PWC, daily precipitation and soil moisture for the seven agricultural plots. Note that several parameters drop to zero because the plants had already been harvested when the last measurement was made.

Behavior of the SAR parameters and effect of the incidence angle

Backscattering coefficients

The temporal evolution of the backscattering coefficients in the linear basis (i.e., HH, HV and VV) and the HH/VV and HV/VV ratios are plotted in Figures 3-7, respectively, for the four crop types and the three incidence angles. At an early time (DoY=45-70), the three backscattering coefficients showed a decreasing trend from very large values. Because the vegetation was very short at that moment, the only explanation of this radar response could be the rain events that occurred during this time period, followed by dry weather (Figure 2). HH (Figure 3) and VV (Figure 4) have very similar values (i.e., HH/VV is approximately 0 dB), and HV is between 5 and 12 dB below the co-polar

channels, as expected from the dominant surface scattering. In fact, the small perturbation model and the Bragg scattering model for rough surfaces predict that VV will be slightly higher than HH, in a range of 0 to 3 dB depending on roughness, moisture and incidence angle (Chen and Fung 1988; Fung 1994; Hajnsek et al. 2003). However, in this study it was measured a very similar backscattering level for both linear channels, as it was also observed at the beginning of the cropping season by other authors in the past (Bouvet et al. 2009; Satalino et al. 2009).

Plants emerged during the intermediate dates (DoY=71-135), and the response of HH increased significantly due to the presence of vertical stems and tillers. However, the response of VV decreased for all crops, especially for 36° and 31°, because the vertical polarization was more attenuated than the horizontal one. This pattern is well described by the HH/VV ratio. At the end of the cycle, from DoY=140 to the end, plants lose their verticality and become randomly oriented, so the difference between the two polarization channels is much smaller, i.e., within +/- 1.5 dB at 36° for most crops. A similar effect occurred for 25°, although high values of both copolar channels could be observed for wheat (L7) during the late dates at this incidence angle, possibly because a higher amount of biomass was present during these stages, as shown in Figure 2.

Figure 5 displays that the cross-polar channel (HV) was mostly driven by the presence of the vegetation volume as it is composed of randomly oriented elements. As previously mentioned, the cross-polar return was very low at all incidence angles during the early dates, but volume scattering increased at intermediate dates (DoY=71-135) because of plant development, so HV increased for all crops and for all three incidence angles. The maximum values (between -13 dB and -14 dB) at this stage are found for

barley (M9) at all incidence angles. It decreased for some crops at the late dates, but in other cases it increased slightly due to the random volume morphology of the crops.

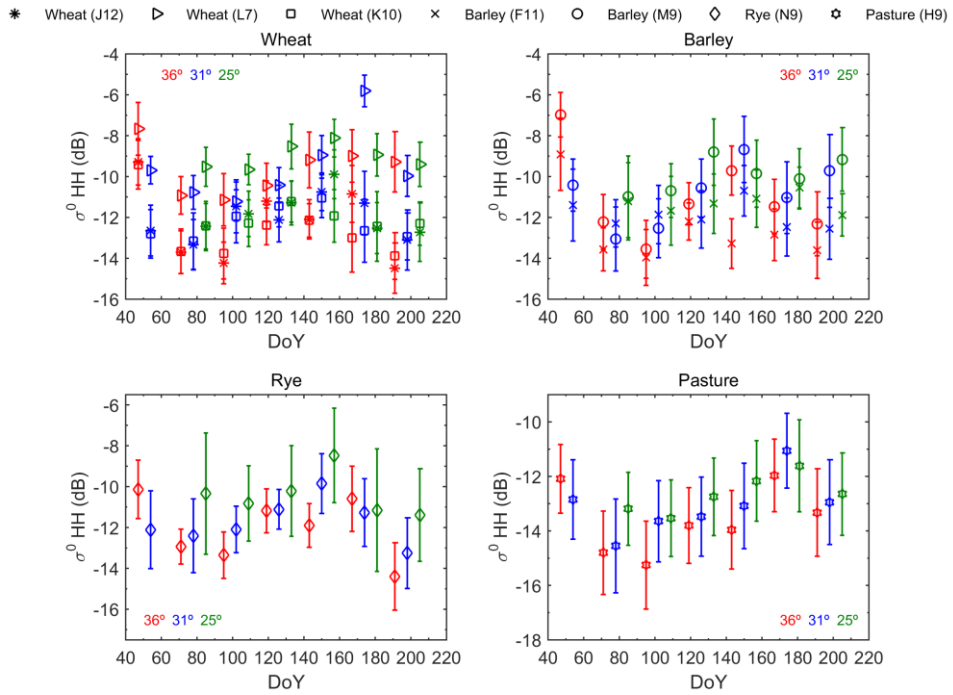

Figure 3. Temporal evolution of the backscattering coefficient (HH) on the linear polarization basis for all fields. Averages (symbols) and standard deviations (error bars) are computed within each field. Red colour denote incidence angle at 36°, blue at 31° and green at 25°.

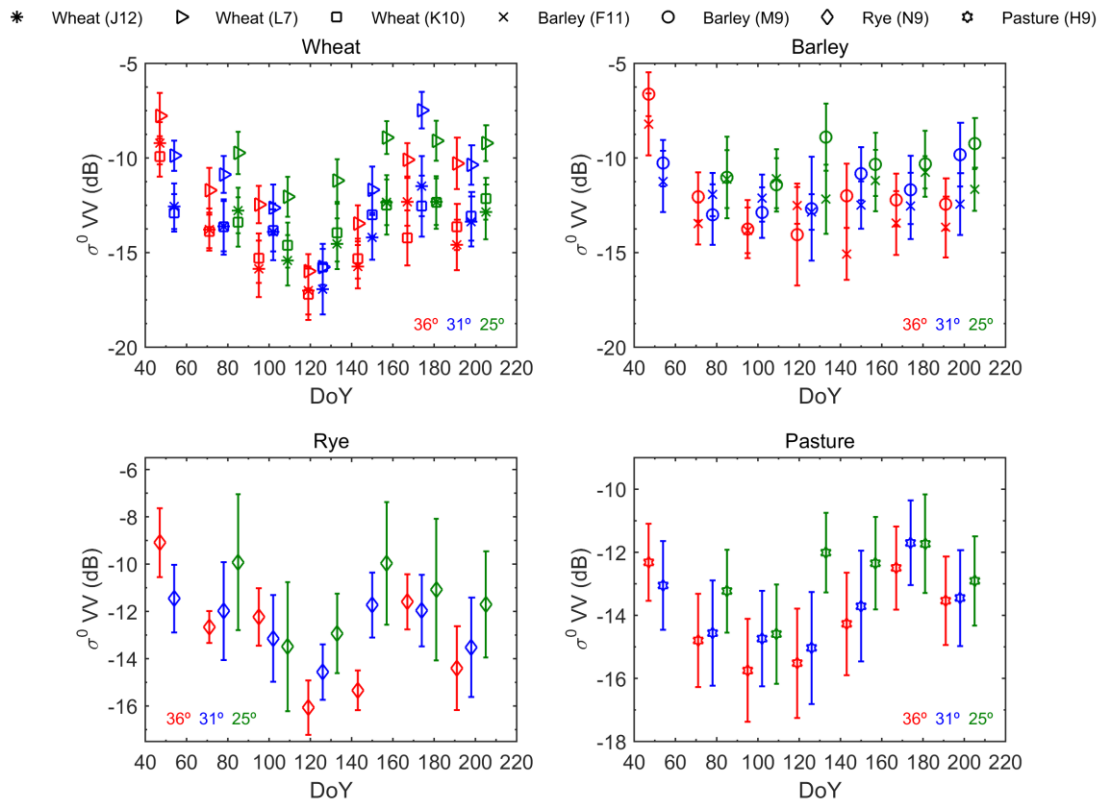

Figure 4. Temporal evolution of the backscattering coefficient (VV) on the linear polarization basis for all fields. Averages (symbols) and standard deviations (error bars) are computed within each field. Red colour denote incidence angle at 36°, blue at 31° and green at 25°.

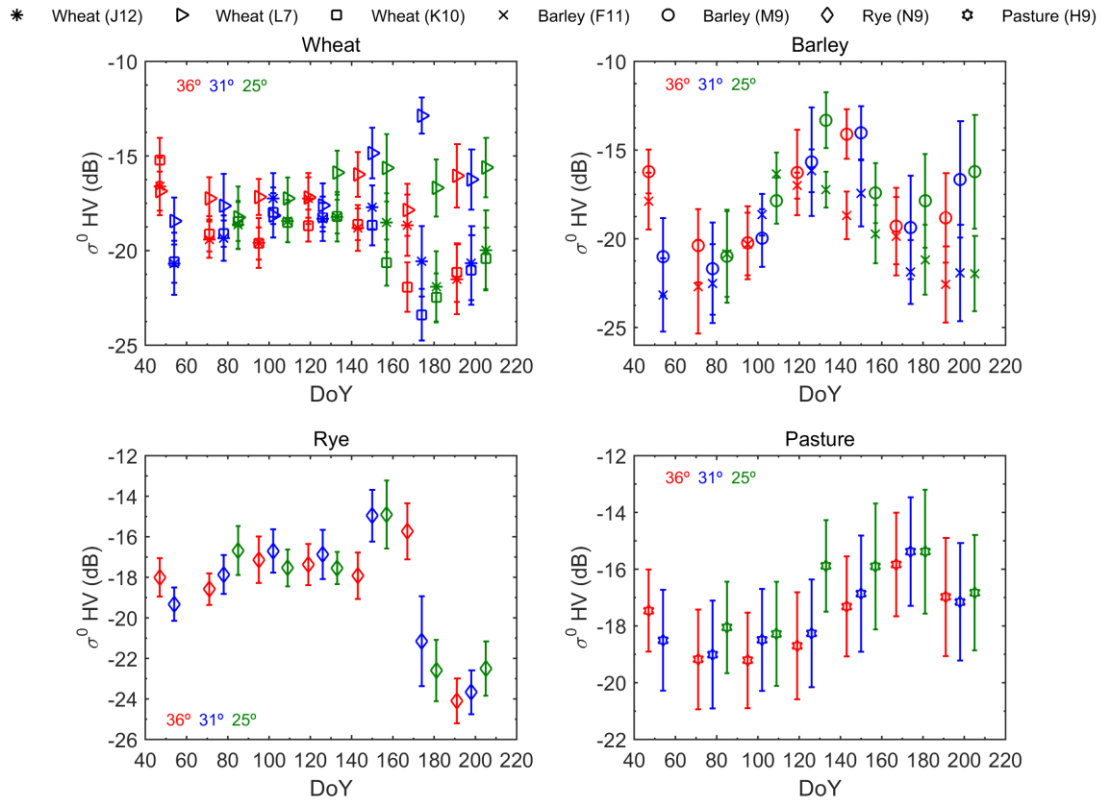

Figure 5. Temporal evolution of the backscattering coefficient (HV) on the linear polarization basis for all fields. Averages (symbols) and standard deviations (error bars) are computed within each field. Red colour denote incidence angle at 36°, blue at 31° and green at 25°.

The co-polar ratio (HH/VV) is strongly sensitive to the crop growth cycle for wheat, barley and rye, whereas it showed quite a uniform response for pasture (Figure 6). The maximum values of this ratio are reached at the middle of the growing season, and clearly depend on the crop type and the incidence angle. The extreme values for wheat and rye are approximately 5 dB both at 31° and 36°, and 2-3 dB at 25°, but the ratio for barley reaches only 2 dB for 31° and 36° and does not show any peak at 25°.

Finally, the HV/VV ratio (Figure 7) also showed an increasing-decreasing behavior with time like the HH/VV ratio, but the values at each date are different for different crops and incidence angles. The shallowest angle (36°) produced the highest

values at each date and the steepest (25°) the smallest ones, with a difference between 2 and 4 dB. Barley is the crop type with the lowest HV/VV values, and both rye and wheat behave similarly. In addition, both ratios have a temporal pattern similar to those of LAI and biomass (Figure 2), suggesting their feasibility for monitoring crop vigor.

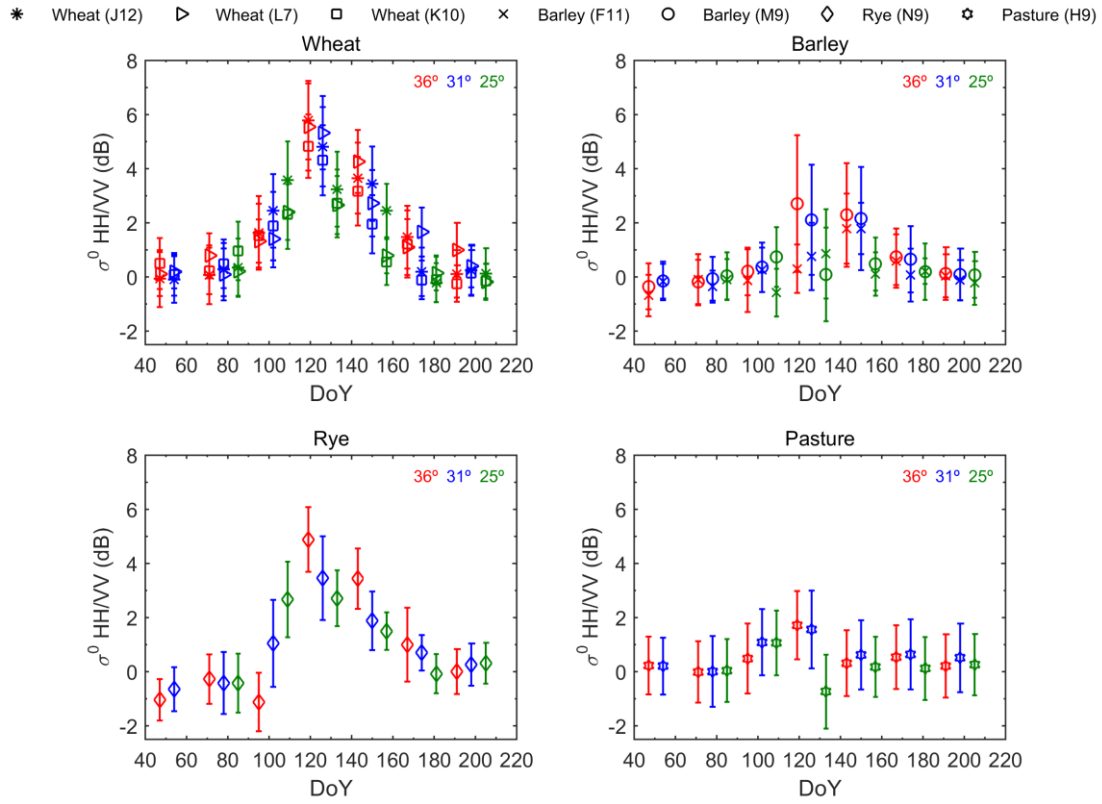

Figure 6. Temporal evolution of the backscattering ratio (HH/VV) on the linear polarization basis for all fields. Averages (symbols) and standard deviations (error bars) are computed within each field. Red colour denote incidence angle at 36°, blue at 31° and green at 25°.

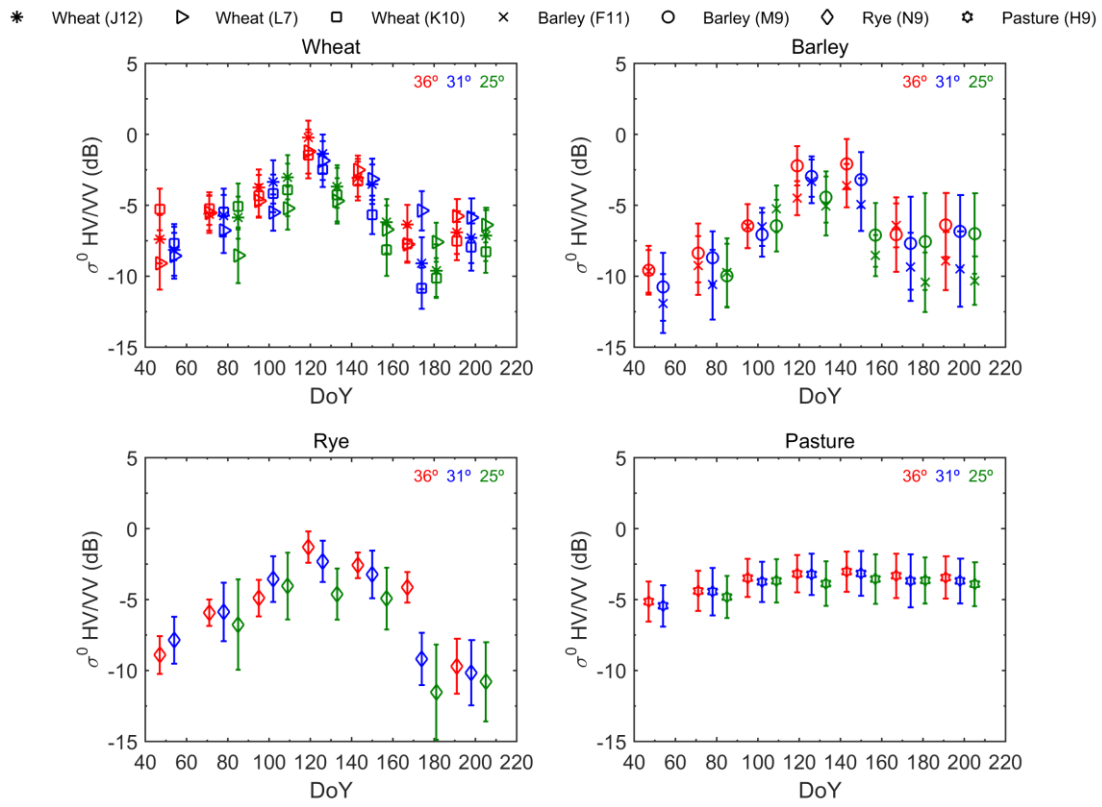

Figure 7. Temporal evolution of the backscattering ratio (HV/VV) on the linear polarization basis for all fields. Averages (symbols) and standard deviations (error bars) are computed within each field. Red colour denote incidence angle at 36°, blue at 31° and green at 25°.

Correlation between HH and VV

Figure 8 depicts the normalized correlation, or coherence, between HH and VV, γ_{HHVV}, for all plots at different incidence angles. During the early stages, when surface scattering is the most important contribution, a high correlation is found, with values between 0.6 and 0.9. Then, as plant foliage develops, γ_{HHVV} decreases between 0.2 and 0.6, depending on the crop type and the incidence angle. In general, the drop is less pronounced at 25° than at 31° and 36°, in agreement with the more pronounced contribution from the soil at steep angles than at shallow angles. At the end of the experiment, coinciding with the driest stage of plants and the harvest time, γ_{HHVV} becomes high again, similar to the beginning of the campaign. The cause of the high

γ_{HHVV} at these late stages is again the dominance of surface scattering, since backscattering from vegetation is reduced due to the dry conditions of the plants. The temporal pattern of γ_{HHVV} is opposite to that of HH/VV and HV/VV ratios, so it suggests an inverse relationship with LAI and biomass (Figure 2).

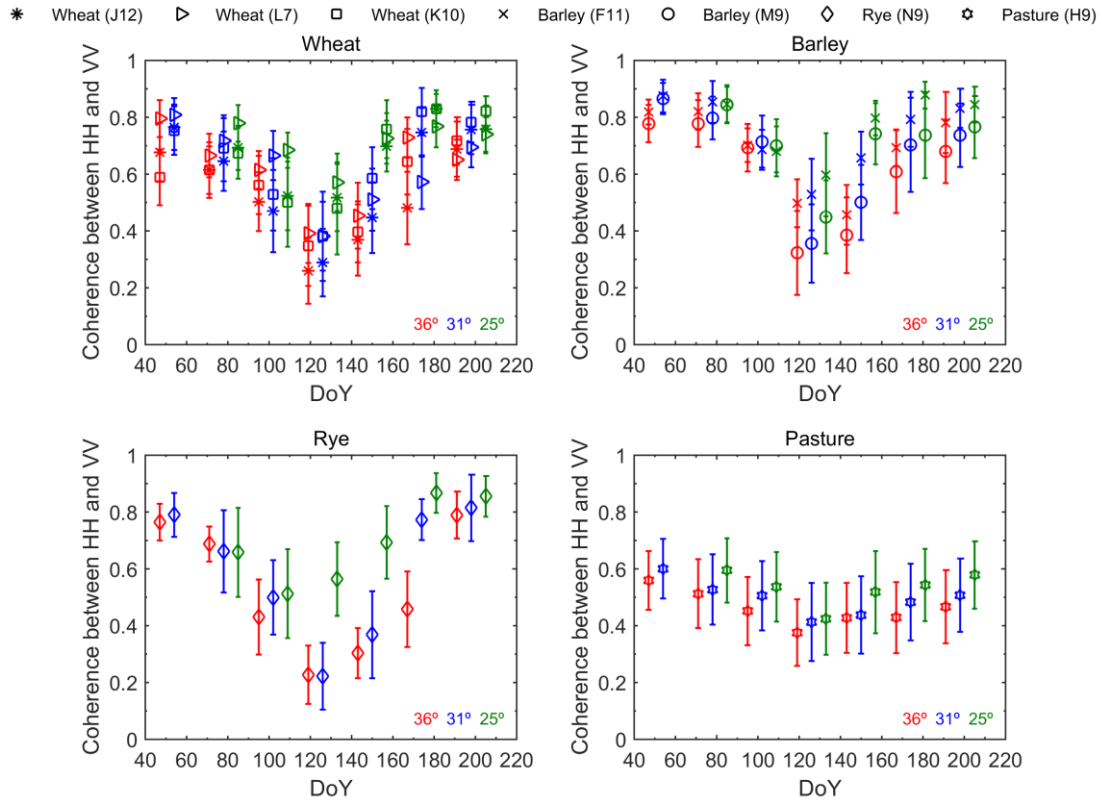

Figure 8. Temporal evolution of the correlation between HH and VV (γ_{HHVV}) for all monitored fields. Averages (symbols) and standard deviations (error bars) are computed within each field. Red colour denote incidence angle at 36°, blue at 31° and green at 25°.

The dominant alpha angle

Figure 9 shows the evolution of the dominant alpha angle (α_1), i.e., the alpha angle of the 1st eigenvector. During the early vegetative phase, α_1 was close to 0° for all crops and angles, which is typical for bare soils and surface scattering. An increasing trend ensued as the plants developed, and peaked at approximately DoY=110-130 with a value of 40° for wheat and rye, at incidence angles of 31° and 36°. This alpha value

corresponds to a linearly polarized radar return resulting from the dominance of HH over VV (HH was 5 dB higher than VV). At the same stage, but at steeper incidence angles (25°), α_1 was only approximately 20°, which means that the dominant scattering mechanism was mostly surface scattering. At the end of the campaign, α_1 decreased, again becoming close to 0° for all incidence angles at harvest time. Once again, the dominant $\alpha_1$evolution follows a time pattern similar to that of LAI and biomass.

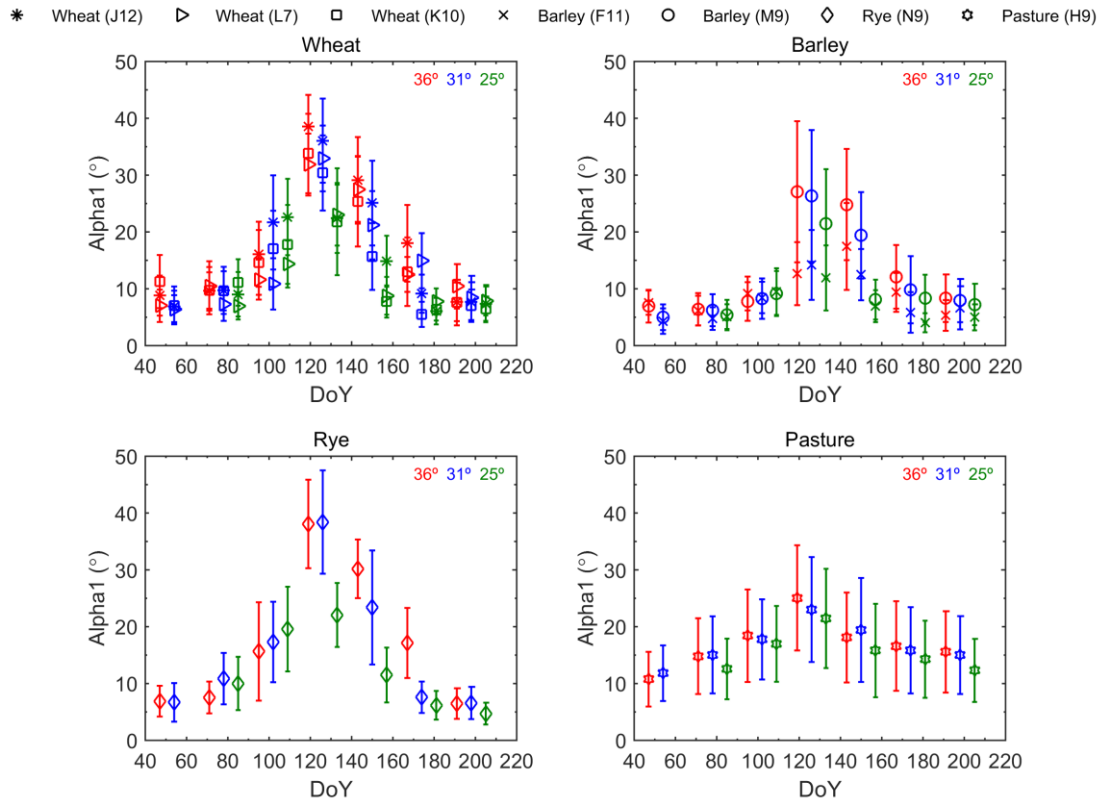

Figure 9. Temporal evolution of the dominant alpha angle (α_1) for all monitored fields. Averages (symbols) and standard deviations (error bars) are computed within each field. Red colour denote incidence angle at 36°, blue at 31° and green at 25°.

Correlation between radar parameters and biophysical variables

The correlation between the backscattering coefficients at the linear basis and the biophysical variables was first analysed. HH (Table 3) is moderately correlated with the scene properties, showing a high correlation only in a few cases. The radar response of

this channel is affected by both vegetation and soil parameters, and as previously discussed, it does not show a consistent temporal pattern (Figure 3). The highest correlation coefficients were obtained for rye for height, PWC and SM, at 25° and 31°, and for wheat (L7) for PWC, the LAI and FVC at incidence angles of 31° and 36°.

VV is highly correlated with biomass for most crops and incidence angles, with the best values at 31° (Table 4). The LAI is also well correlated with VV, especially at 31° for most crops and at 36° for wheat. These two plant parameters are significantly but negatively correlated with VV because an increase in biomass or LAI translates into a stronger attenuation of the vertically polarized waves and a consequent decrease in VV (Figure 4). The most consistent results for VV are obtained at 31°, with lower correlations at 25° and 36°, so this angle seems to be a good choice at this frequency band to monitor crop development.

The correlations for HV (Table 5) are not as good as expected in regard of previous results found in the literature (Moran et al. 2012). It is only moderately correlated to vegetation height and biomass at 31° for most crop types. Both biophysical variables are related to an increase in the vegetation volume, and volume scattering is known to generate significant backscattering in the cross-polarized channel. The rest of the biophysical variables evidence many inconsistencies in the correlations, with opposite signs for different fields of the same crop (e.g., for FVC for wheat at 25° and 31°, or for SM at 25°), making difficult any physical interpretation.

The physical parameters related to water content (i.e., SM and PWC) show no correlation with the backscattering coefficients (excepting some isolated high values), whereas those related to scene geometry or morphology (i.e., height, biomass and LAI) exhibit better correlation coefficients.

Regarding the incidence angle, the intermediate angle (31°) provides the best correlations, probably because it results in a trade-off between the soil dominance at 25° and an excessive attenuation within the vegetation at 36°.

As some fluctuations of the backscattering coefficients are common to different polarization channels (probably due to specific events such as rain or other external sources), it is expected that the effect of such variations will be minimized if backscattering ratios are employed, such as HH/VV and HV/VV. These ratios exhibit high correlations with biophysical variables in many cases. Tables 6 and 7 indicates that the strongest correlations for these ratios were observed with biomass for all crops, and most notably at 31° and 36°, with very high values and positive correlations. In agreement with these results, the C-band copolar ratio HH/VV was found to be highly correlated with biomass for winter wheat at a 40° incidence angle by Mattia et al. (2003), whereas the correlation was poor at 23°. Moreover, Moran et al. (2012) also reported a very good correlation of VV/HH (i.e., the inverse of HH/VV) with crop growth for winter barley at an incidence angle greater than 35°. Both HH/VV and HV/VV are also highly correlated with vegetation height and moderately correlated with LAI, supporting the previous insights found in the temporal evolution analysis.

The correlation of γ_{HHVV} with biomass is high for all crops, and moderate to high with height for all crops at incidence angles of 31° and 36° (Table 8). These correlations are negative because of the temporal pattern of γ_{HHVV} in the presence of crops (Figure 8), as it was previously discussed: high when surface scattering is dominant (i.e., at early and late dates) and low when vegetation is present (i.e., in the middle of the season).

In the same fashion as the backscattering ratios and γ_{HHVV}, α_1 is highly correlated with biomass for all crops at incidence angles of 31° and 36° (Table 9).

Indeed, the physical reason for this correlation is the same: the gradual change of the scattering mechanism that dominates the radar response of the crops during the growth cycle (see Figure 9). Consequently, it follows the typical curve for biomass, as shown in Figure 2. Lopez-Sanchez et al. (2013) used this principle and employed the α_1 to estimate the phenological stage of several crops.

It is remarkable that occasionally, fluctuating and even inverse correlations have been found between plots with the same crop. Those few cases took place mainly over wheat plots and for the shallower angles, and can be justified by a higher variability between wheat evolutions than for barley (Figure 2).

Table 3. Correlation (r Pearson) between the field measurements and the co-polar channel HH, for the three incidence angles (i.e., 25°, 31° and 36°). Significant correlations at 95% coincidence level are shaded.

	Height			Biomass			PWC			LAI			FVC			SM		
	25°	31°	36°	25°	31°	36°	25°	31°	36°	25°	31°	36°	25°	31°	36°	25°	31°	36°
J12 (Wheat)	0.76	0.57	0.27	0.71	0.47	0.25	-0.50	-0.58	-0.33	0.32	0.03	0.00	0.39	0.02	-0.28	-0.44	-0.01	0.48
L7 (Wheat)	-0.48	0.53	0.24	-0.69	-0.21	-0.31	0.27	-0.83	-0.40	-0.54	-0.77	-0.75	-0.25	-0.92	-0.77	0.52	0.24	0.18
K10 (Wheat)	-0.64	0.75	-0.19	-0.4	0.67	0.02	0.46	-0.52	0.16	-0.29	0.04	-0.22	-0.04	-0.64	-0.37	0.65	-0.29	0.53
F11 (Barley)	-0.39	0.36	-0.28	-0.53	-0.11	-0.12	-0.28	-0.56	-0.18	-0.48	-0.31	-0.06	-0.51	-0.29	-0.10	0.71	0.14	0.68
M9 (Barley)	-0.44	0.58	0.15	-0.51	0.37	0.01	0.31	-0.48	-0.03	-0.37	-0.31	-0.30	-0.32	-0.40	-0.32	0.51	0.11	0.29
N9 (Rye)	0.82	0.95	0.30	0.44	0.34	-0.18	-0.76	-0.83	-0.39	-0.21	-0.61	-0.69	-0.24	-0.52	-0.65	-0.78	-0.72	0.16
H9 (Pasture)	-0.44	0.26	0.35	-0.50	-0.19	-0.15	0.21	-0.41	-0.46	-0.42	-0.36	-0.32	-0.02	-0.53	-0.61	0.83	0.43	0.43

Table 4. Correlation (r Pearson) between field measurements and the co-polar channel VV, for the three incidence angles (i.e., 25°, 31° and 36°). Significant correlations at 95% coincidence level are shaded.

	Height			Biomass			PWC			LAI			FVC			SM		
	25°	31°	36°	25°	31°	36°	25°	31°	36°	25°	31°	36°	25°	31°	36°	25°	31°	36°
J12 (Wheat)	-0.62	-0.45	-0.42	-0.67	-0.70	-0.61	0.24	-0.21	-0.14	-0.58	-0.80	-0.76	-0.65	-0.82	-0.87	0.50	0.62	0.66
L7 (Wheat)	-0.61	-0.25	-0.38	-0.84	-0.80	-0.87	0.31	-0.26	-0.09	-0.57	-0.72	-0.75	-0.18	-0.45	-0.40	0.60	0.50	0.52
K10 (Wheat)	-0.63	-0.30	-0.63	-0.59	-0.80	-0.72	0.30	-0.25	0.22	-0.49	-0.77	-0.61	-0.10	-0.46	-0.13	0.65	0.41	0.57
F11 (Barley)	0.44	-0.59	-0.57	0.43	-0.79	-0.36	0.16	-0.16	-0.04	0.34	-0.62	-0.17	0.37	-0.63	-0.21	-0.62	0.60	0.76
M9 (Barley)	-0.49	-0.05	-0.34	-0.55	-0.26	-0.51	0.33	-0.23	0.07	-0.38	-0.61	-0.63	-0.33	-0.64	-0.58	0.52	0.49	0.56
N9 (Rye)	-0.56	-0.11	-0.46	-0.87	-0.83	-0.87	0.37	-0.19	0.09	-0.40	-0.53	-0.21	-0.46	-0.78	-0.53	0.34	-0.22	0.23
H9 (Pasture)	-0.54	-0.03	0.11	-0.45	-0.59	-0.51	0.36	-0.47	-0.51	-0.33	-0.71	-0.62	0.14	-0.61	-0.69	0.82	0.65	0.55

Table 5. Correlation (r Pearson) between the field measurements and the cross-polar channel HV, for the three incidence angles (i.e., 25°, 31° and 36°). Significant correlations at 95% coincidence level are shaded.

	Height			Biomass			PWC			LAI			FVC			SM		
	25°	31°	36°	25°	31°	36°	25°	31°	36°	25°	31°	36°	25°	31°	36°	25°	31°	36°
J12 (Wheat)	0.49	0.48	0.01	0.64	0.62	0.18	0.08	-0.02	0.15	0.57	0.60	0.37	0.75	0.79	0.10	-0.83	-0.70	0.33
L7 (Wheat)	0.54	0.80	0.21	0.09	0.14	0.21	-0.50	-0.93	0.12	-0.55	-0.55	-0.13	-0.77	-0.82	-0.11	-0.11	-0.20	-0.64
K10 (Wheat)	-0.77	0.22	-0.56	-0.39	0.59	-0.01	0.67	0.27	0.69	-0.12	0.62	0.10	0.17	0.32	0.18	0.58	-0.68	0.30
F11 (Barley)	0.43	0.45	0.21	0.60	0.85	0.71	0.25	0.25	0.12	0.54	0.79	0.72	0.57	0.82	0.72	-0.69	-0.61	-0.08
M9 (Barley)	-0.36	0.94	0.69	-0.41	0.86	0.65	0.29	-0.50	-0.10	-0.29	0.20	0.26	-0.25	0.10	0.20	0.47	-0.43	-0.35
N9 (Rye)	0.61	0.62	0.59	0.69	0.64	0.24	-0.47	-0.28	-0.77	0.24	0.13	-0.08	0.25	0.25	-0.35	-0.58	-0.74	-0.27
H9 (Pasture)	-0.47	0.68	0.63	-0.43	-0.09	-0.16	0.31	-0.89	-0.84	-0.33	-0.36	-0.39	0.08	-0.92	-0.92	0.80	-0.10	0.02

Table 6. Correlation (r Pearson) between field measurements and the co-polar ratio HH/VV, for the three incidence angles (i.e., 25°, 31° and 36°). Significant correlations at 95% coincidence level are shaded.

	Height			Biomass			PWC			LAI			FVC			SM		
	25°	31°	36°	25°	31°	36°	25°	31°	36°	25°	31°	36°	25°	31°	36°	25°	31°	36°
J12 (Wheat)	0.68	0.73	0.67	0.70	0.92	0.88	-0.35	-0.11	-0.06	0.49	0.76	0.89	0.56	0.79	0.82	-0.48	-0.59	-0.44
L7 (Wheat)	0.70	0.72	0.59	0.93	0.86	0.88	-0.34	-0.30	-0.11	0.55	0.33	0.50	0.09	-0.13	0.06	-0.64	-0.46	-0.53
K10 (Wheat)	-0.45	0.60	0.64	0.08	0.94	0.89	0.60	-0.06	-0.15	0.19	0.60	0.59	0.07	0.03	-0.11	0.42	-0.45	-0.32
F11 (Barley)	-0.42	0.83	0.84	-0.46	0.60	0.63	-0.19	-0.35	-0.21	-0.39	0.27	0.28	-0.42	0.30	0.31	0.65	-0.41	-0.58
M9 (Barley)	0.55	0.96	0.84	0.61	0.92	0.93	-0.36	-0.44	-0.17	0.40	0.33	0.66	0.34	0.23	0.56	-0.53	-0.48	-0.54
N9 (Rye)	0.64	0.67	0.59	0.84	0.86	0.76	-0.47	-0.36	-0.27	0.30	0.04	-0.12	0.35	0.28	0.22	-0.44	-0.28	-0.15
H9 (Pasture)	0.56	0.53	0.44	0.44	0.82	0.87	-0.40	0.18	0.27	0.31	0.74	0.78	-0.18	0.24	0.37	-0.82	-0.50	-0.41

Table 7. Correlation (r Pearson) between field measurements and the cross-polar ratio HV/VV for the three incidence angles (i.e., 25°, 31° and 36°). Significant correlations at 95% coincidence level are shaded.

	Height			Biomass			PWC			LAI			FVC			SM		
	25°	31°	36°	25°	31°	36°	25°	31°	36°	25°	31°	36°	25°	31°	36°	25°	31°	36°
J12 (Wheat)	0.61	0.52	0.43	0.68	0.75	0.70	-0.20	0.13	0.21	0.58	0.81	0.93	0.68	0.91	0.94	-0.55	-0.73	-0.55
L7 (Wheat)	0.76	0.83	0.39	0.89	0.86	0.84	-0.44	-0.45	0.10	0.46	0.27	0.66	0.00	-0.19	0.35	-0.65	-0.62	-0.61
K10 (Wheat)	-0.70	0.27	0.18	-0.10	0.73	0.76	0.84	0.28	0.38	0.28	0.74	0.74	0.38	0.41	0.30	0.35	-0.60	-0.35
F11 (Barley)	0.41	0.49	0.61	0.70	0.87	0.82	0.31	0.24	0.12	0.66	0.78	0.68	0.69	0.81	0.71	-0.70	-0.63	-0.65
M9 (Barley)	0.42	0.90	0.80	0.44	0.91	0.90	-0.03	-0.36	-0.13	0.30	0.45	0.67	0.22	0.37	0.59	-0.02	-0.61	-0.69
N9 (Rye)	0.60	0.46	0.67	0.81	0.85	0.91	-0.43	-0.08	-0.39	0.33	0.35	0.16	0.37	0.57	0.36	-0.47	-0.37	-0.32
H9 (Pasture)	0.66	0.85	0.80	0.49	0.60	0.60	-0.46	-0.50	-0.46	0.33	0.43	0.42	-0.25	-0.35	-0.30	-0.85	-0.90	-0.89

Table 8. Correlation (r Pearson) between field measurements and the normalized correlation (coherence) between HH and VV (γ_{HHVV}) for the three incidence angles (i.e., 25°, 31° and 36°). Significant correlations at 95% coincidence level are shaded.

	Height			Biomass			PWC			LAI			FVC			SM		
	25°	31°	36°	25°	31°	36°	25°	31°	36°	25°	31°	36°	25°	31°	36°	25°	31°	36°
J12 (Wheat)	-0.60	-0.64	-0.77	-0.76	-0.85	-0.92	0.07	0.00	0.20	-0.76	-0.81	-0.81	-0.84	-0.86	-0.76	0.60	0.65	0.45
L7 (Wheat)	0.54	-0.83	-0.49	0.55	-0.84	-0.87	-0.42	0.47	-0.01	0.30	-0.23	-0.59	0.04	0.22	-0.23	-0.49	0.53	0.61
K10 (Wheat)	0.32	-0.49	-0.54	-0.29	-0.86	-0.92	-0.61	-0.04	0.00	-0.42	-0.66	-0.57	-0.16	-0.10	0.03	-0.23	0.48	0.39
F11 (Barley)	0.31	-0.39	-0.54	-0.14	-0.90	-0.88	-0.14	-0.32	-0.21	-0.28	-0.86	-0.76	-0.26	-0.88	-0.78	-0.28	0.57	0.64
M9 (Barley)	0.43	-0.89	-0.85	0.47	-0.94	-0.93	-0.34	0.26	0.20	0.30	-0.55	-0.65	0.25	-0.47	-0.54	-0.47	0.56	0.54
N9 (Rye)	-0.52	-0.60	-0.67	-0.85	-0.88	-0.88	0.32	0.24	0.41	-0.43	-0.16	-0.22	-0.49	-0.42	-0.34	0.38	0.37	0.36
H9 (Pasture)	0.44	-0.86	-0.78	0.33	-0.66	-0.77	-0.39	0.44	0.27	0.22	-0.53	-0.60	-0.16	0.31	0.11	-0.74	0.89	0.81

Table 9. Correlation (r Pearson) between field measurements and the dominant alpha angle, α_1, for the three incidence angles (i.e., 25°, 31° and 36°). Significant correlations at 95% coincidence level are shaded.

	Height			Biomass			PWC			LAI			FVC			SM		
	25°	31°	36°	25°	31°	36°	25°	31°	36°	25°	31°	36°	25°	31°	36°	25°	31°	36°
J12 (Wheat)	0.69	0.70	0.72	0.73	0.90	0.92	-0.30	-0.06	-0.12	0.56	0.81	0.85	0.63	0.82	0.78	-0.51	-0.58	-0.43
L7 (Wheat)	-0.58	0.76	0.63	-0.56	0.82	0.86	0.45	-0.35	-0.15	-0.29	0.25	0.42	-0.01	-0.19	-0.01	0.51	-0.47	-0.53
K10 (Wheat)	-0.65	0.54	0.61	-0.26	0.92	0.92	0.58	0.00	-0.10	-0.09	0.65	0.59	0.04	0.10	-0.08	0.60	-0.44	-0.31
F11 (Barley)	-0.25	0.54	0.65	0.19	0.90	0.78	0.12	0.20	0.04	0.30	0.77	0.58	0.28	0.79	0.61	0.24	-0.61	-0.64
M9 (Barley)	-0.47	0.90	0.83	-0.51	0.92	0.92	0.35	-0.22	-0.13	-0.33	0.52	0.63	-0.27	0.45	0.53	0.49	-0.53	-0.52
N9 (Rye)	0.29	0.52	0.60	0.69	0.88	0.86	0.04	-0.16	-0.28	0.25	0.15	0.12	0.49	0.46	0.36	-0.01	-0.22	-0.21
H9 (Pasture)	-0.36	0.78	0.54	-0.21	0.81	0.87	0.42	-0.20	0.12	-0.11	0.72	0.80	0.19	-0.07	0.28	0.67	-0.90	-0.72

Because of the great number of correlations resulting from the possible combinations between parameters, field observations and incidence angles, Table 10 summarizes the correlation results, indicating the best correlations ($r \geq +/-0.66$) and the recommended incidence angle for each biophysical variable and SAR parameter.

Table 10. Overview of SAR parameters and highly-correlated biophysical variables taking into account the incidence angle for all crops analyzed in this study. A check mark is used to show the best combinations.

	Height		Biomass		LAI	
	31°	36°	31°	36°	31°	36°
HH						
HV						
VV						
HH/VV	✓	✓	✓	✓		
HV/VV	✓	✓	✓	✓	✓	✓
γ_{HHVV}	✓	✓	✓	✓		
α_1			✓	✓		

This correlation study allows us to identify relationships between radar parameters and field parameters, although it should be carefully considered due to the limited number of field observations. The scarcity of ground measurements is a recurrent and steady issue in radar applications. The literature contains many examples of correlation analyses with a similar (or smaller) number of ground observations against radar estimates. Maity et al. (2004) compared three field measurements with RADARSAT for cotton parametrization in India during low to peak crop growth stages. Lim et al. (2008) carried out a temporal study with multiple angles comparing six rice parameters with ground-based C-band scatterometer measurements for an entire growing season, with a similar objective as the present study. Kim et al. (2012) compared radar-derived vegetation indices of rice and soybean (12~19 measurements) to estimate VWC. Baghdadi et al. (2016) used 18 field measurements to characterize irrigated grasslands, and used polarimetric RADARSAT-2 data at different incidence

angles. Field measurements are highly time-consuming, and it is typically difficult to gather a comprehensive dataset of *in situ* data.

Potential applications

The results presented in previous section suggest a number of potential applications of the radar parameters. First, all the rainfed crops analyzed here respond quite similarly, but in a different manner than the natural pasture. Thus, it may be inferred than cereals can be distinguished from natural pasture or grassland areas by exploiting the single radar parameters considered here at any incidence angle. Second, the HH/VV and HV/VV ratios, α_1, and γ_{HHVV} capture the dynamics of the growth cycle of these crops well at both 31° and 36°. Therefore, a time series of these observations could be used as input for monitoring products and applications such as the detection of cultivation problems, and forecasting dates for key treatments (e.g., fertilization) or harvest. These applications could be set up by interleaving both 31° and 36° incidence series, which would increase the information refresh rate, thus improving its applicability -an important aspect for end users. In this context, it should be emphasized that the HV/VV ratio, which is very sensitive to plant development, is freely available on a routine basis over Europe with a revisit time of 6 days since 2016, thanks to the constellation of Sentinel-1A and 1B. The use of dual-pol modes such as for Sentinel-1A and 1B provides better spatial coverage (i.e., a double swath) with respect to quad-pol images, at the expense of a reduced polarimetric observation space. In addition, the revisit time (i.e., the refresh rate) is a key aspect which may favor systems with less polarimetric channels when timeliness is relevant. In the same vein, a deep analysis on the best combination of channels in a dual-pol system should be carried out considering the application objectives.

In this study it was obtained very significant correlations of some parameters with height and biomass, which opens the door for the development of Earth Observation products based on the estimation of these parameters. Biomass is known to be related to crop yield, so a yield forecast based on a time series of C-band radar data (e.g., from Sentinel-1) is possible. In addition, data fusion with optical data (especially those provided by Sentinel-2) could be explored to take advantage of their complementarity. Radar data are sensitive to the structure and morphology of the canopy, whereas optical data are more sensitive to the biochemistry related to the plants physiological activity. This synergy has been recently exploited for crop monitoring in a data fusion framework (De Bernardis et al. 2016).

Additionally, further research may account for a full regression model based on the best relationships found here in order to retrieve and validate a complete dataset of vegetation parameters.

Conclusions

This study aimed to assess the feasibility of several polarimetric parameters at different incidence angles to crop monitor through the analysis of their relationship with different plant and canopy biophysical variables. The SAR response for many of the polarimetric parameters suggested a temporal pattern similar to that of the LAI and biomass, confirmed with the correlation analysis. The most significant correlations were observed for the backscattering ratios (HH/VV and HV/VV), the normalized correlation between HH and VV (γ_{HHVV}) and the dominant alpha angle (α_1) with biomass, height and the LAI at 31° and 36° incidence angles.

Regarding the impact of the incidence angle, the angle of 31° provides the best results. The radar waves travel more vertically at 25°, so the scattering at steeper

incidence angles is more influenced by the soil properties, whereas the radar waves travel a longer path through the vegetation at 36°.

The results of this research may provide some insight on the selection of polarimetric parameters as a remotely sensed alternative to crop monitoring. It was shown that biomass, LAI and height of rainfed crops may be surveyed using different radar parameters provided by RADARSAT-2, even though additional field campaigns are needed to confirm these results over different areas and crops. Given the improved spatial resolution of recent missions, including RADARSAT-2 and Sentinel-1, and the future RADARSAT Constellation Mission (RCM), and their large availability of data, the use of radar imagery is nowadays a confirmed foundation for agricultural applications at plot scale.

Acknowledgments

This study was supported by the Spanish Ministry of Economy and Competitiveness, MINECO (Projects ESP2015-67549-C3-3, ESP2017-89463-C3-3-R, and TEC2017-85244-C2-1-P) and the European Regional Development Fund, FEDER. RADARSAT-2 Data and Products @ MacDonald, Dettwiler and Associates Ltd. (MDA, 2015) – All Rights Reserved. RADARSAT is an official trademark of the Canadian Space Agency (CSA). All RADARSAT-2 images have been provided by MDA and CSA in the framework of the SOAR-EU2 Project ref. 16375.

References

Adams, J.R., Berg, A.A., McNairn, H., and Merzouki, A. 2013a. "Sensitivity of C-band SAR polarimetric variables to unvegetated agricultural fields." *Canadian Journal of Remote Sensing*, Vol. 39(No. 1): pp. 1-16. doi:10.5589/m13-003.

Adams, J.R., Rowlandson, T.L., McKeown, S.J., Berg, A.A., McNairn, H., and Sweeney, S.J. 2013b. “Evaluating the Cloude-Pottier and Freeman-Durden scattering decompositions for distinguishing between unharvested and post-harvest agricultural fields.” *Canadian Journal of Remote Sensing*, Vol. 39(No. 4): pp. 318-327. doi:10.5589/m13-040.

Baghdadi, N.N., El Hajj, M., Zribi, M., and Fayad, I. 2016. “Coupling SAR C-band and optical data for soil moisture and leaf area index retrieval over irrigated grasslands.” *IEEE Journal of Selected Topics in Applied Earth Observations and Remote Sensing*, Vol. 9(No. 3): pp. 1229-1243. doi:10.1109/JSTARS.2015.2464698.

Bériaux, E., Waldner, F., Collienne, F., Bogaert, P., and Defourny, P. 2015. “Maize leaf area index retrieval from synthetic quad pol SAR time series using the water cloud model.” *Remote Sensing*, Vol. 7(No. 12): pp. 16204-16225. doi:10.3390/rs71215818.

Bouvet, A., Le Toan, T., and Lam-Dao, N. 2009. “Monitoring of the rice cropping system in the Mekong delta using ENVISAT/ASAR dual polarization data.” *IEEE Transactions on Geoscience and Remote Sensing*, Vol. 47(No. 2): pp. 517-526. doi:10.1109/TGRS.2008.2007963.

Brocca, L., Hasenauer, S., Lacava, T., Melone, F., Moramarco, T., Wagner, W., Dorigo, W., et al. 2011. “Soil moisture estimation through ASCAT and AMSR-E sensors: an intercomparison and validation study across Europe.” *Remote Sensing of Environment*, Vol. 115(No. 12): pp. 3390-3408. doi:10.1016/j.rse.2011.08.003.

Cable, J.W., Kovacs, J.M., Jiao, X., and Shang, J. 2014. “Agricultural monitoring in Northeastern Ontario, Canada, using multi-temporal polarimetric RADARSAT-2 data.” *Remote Sensing*, Vol. 6(No. 3): pp. 2343-2371. doi:10.3390/rs6032343.

Ceballos, A., Scipal, K., Wagner, W., and Martínez-Fernández, J. 2005. “Validation of ERS scatterometer-derived soil moisture data in the central part of the Duero Basin, Spain.” *Hydrological Processes*, Vol. 19(No. 8): pp. 1549-1566. doi:10.1002/hyp.5585.

Chen, M.F., and Fung, A.K. 1988. “A numerical study of the regions of validity of the Kirchhoff and small-perturbation rough surface scattering models.” *Radio Science*, Vol. 23(No. 2): pp. 163-170. doi:10.1029/RS023i002p00163.

Cloude, S.R., and Pottier, E. 1997. “An entropy based classification scheme for land applications of polarimetric SAR.” *IEEE Transactions on Geoscience and Remote Sensing*, Vol. 35(No. 1): pp. 68-78. doi:10.1109/36.551935.

Cloude, S.R., and Pottier, E. 1996. “A review of target decomposition theorems in radar polarimetry.” *IEEE Transactions on Geoscience and Remote Sensing*, Vol. 34(No. 2): pp. 498-518. doi:10.1109/36.485127.

Colliander, A., Jackson, T.J., Bindlish, R., Chan, S., Das, N., Kim, S.B., Cosh, M.H. et al. 2017. "Validation of SMAP surface soil moisture products with core validation sites." *Remote Sensing of Environment*, Vol. 191: pp. 215-231. doi:10.1016/j.rse.2017.01.021.

De Bernardis, C., Vicente-Guijalba, F., Martinez-Marin, T., and Lopez-Sanchez, J.M. 2016. “Contribution to real-time estimation of crop phenological states in a dynamical framework based on NDVI time series: data fusion with SAR and temperature.” *IEEE Journal of Selected Topics in Applied Earth Observations and Remote Sensing*, Vol. 9(No. 8): pp. 3512-3523. doi:10.1109/JSTARS.2016.2539498.

Della Vecchia, A., Ferrazzoli, P., Guerriero, L., Blaes, X., Defourny, P., Dente, L., Mattia, F., Satalino, G., Strozzi, T., and Wegmuller, U. 2006. “Influence of

geometrical factors on crop backscattering at C-band." *IEEE Transactions on Geoscience and Remote Sensing*, Vol. 44(No. 4): pp. 778-790. doi:10.1109/TGRS.2005.860489.

Freeman, A., and Durden, S.L. 1998. "A three-component scattering model for polarimetric SAR data." *IEEE Transactions on Geoscience and Remote Sensing*, Vol. 36(No. 3): pp. 963-973. doi:10.1109/36.673687.

Fung, A.K. 1994. "Microwave scattering and emission models and their applications." Norwood, MA: Artech House.

González-Zamora, A., Sánchez, N., and Martínez-Fernández, J. 2016. "Validation of Aquarius soil moisture products over the Northwest of Spain: a comparison with SMOS." *IEEE Journal of Selected Topics in Applied Earth Observations and Remote Sensing*, Vol. 9(No. 6): pp. 2763-2769. doi:10.1109/JSTARS.2016.2517401.

Hajnsek, I., Pottier, E., and Cloude, S.R. 2003. "Inversion of surface parameters from polarimetric SAR." *IEEE Transactions on Geoscience and Remote Sensing*, Vol. 41(No. 4): pp. 727-744. doi:10.1109/TGRS.2003.810702.

Inoue, Y., Kurosu, T., Maeno, H., Uratsuka, S., Kozu, T., Dabrowska-Zielinska, K., and Qi, J. 2002. "Season-long daily measurements of multifrequency (Ka, Ku, X, C, and L) and full-polarization backscatter signatures over paddy rice field and their relationship with biological variables." *Remote Sensing of Environment*, Vol. 81(No. 2-3): pp. 194-204. doi:10.1016/S0034-4257(01)00343-1.

Inoue, Y., and Sakaiya, E. 2013. "Relationship between X-Band backscattering coefficients from high-resolution satellite SAR and biophysical variables in paddy rice." *Remote Sensing Letters*, Vol. 4(No. 3): pp. 288-295. doi:10.1080/2150704X.2012.725482.

Inoue, Y., Sakaiya, E., and Wang, C. 2014. “Capability of C-band backscattering coefficients from high-resolution satellite SAR sensors to assess biophysical variables in paddy rice.” *Remote Sensing of Environment*, Vol. 140: pp. 257-266. doi:10.1016/j.rse.2013.09.001.

Jackson, T.J., Chen, D., Cosh, M., Li, F., Anderson, M., Walthall, C., Doriaswamy, P., and Hunt, E.R. 2004. “Vegetation water content mapping using Landsat data derived normalized difference water index for corn and soybeans.” *Remote Sensing of Environment*, Vol. 92(No. 4): pp. 475-482. doi:10.1016/j.rse.2003.10.021.

Jiang, Z., Huete, A.R., Chen, J., Chen, Y., Li, J., Yan, G., and Zhang, X. 2006. “Analysis of NDVI and scaled difference vegetation index retrievals of vegetation fraction.” *Remote Sensing of Environment*, Vol. 101(No. 3): pp. 366-378. doi:10.1016/j.rse.2006.01.003.

Jiao, X., McNairn, H., Shang, J., Pattey, E., Liu, J., and Champagne, C. 2011. “The sensitivity of RADARSAT-2 polarimetric SAR data to corn and soybean leaf area index.” *Canadian Journal of Remote Sensing*, Vol. 37(No. 1): pp. 69-81. doi:10.5589/m11-023.

Kim, Y., Jackson, T., Bindlish, R., Lee, H., and Hong, S. 2012. “Radar vegetation index for estimating the vegetation water content of rice and soybean.” *IEEE Geoscience and Remote Sensing Letters*, Vol. 9(No. 4): pp. 564-568. doi:10.1109/LGRS.2011.2174772.

Lee, J.S., Ainsworth, T.L., Kelly, J.P., and Lopez-Martinez, C. 2008. “Evaluation and bias removal of multilook effect on entropy/alpha/anisotropy in polarimetric SAR decomposition.” *IEEE Transactions on Geoscience and Remote Sensing*, Vol. 46(No. 10): pp. 3039-52. doi:10.1109/TGRS.2008.922033.

Lim, K.-S., Koo, V.C., and Ewe, H.-T. 2008. “Multi-angular scatterometer measurements for various stages of rice growth.” *Progress In Electromagnetics Research*, Vol. 83: pp. 385-396. doi:10.2528/PIER08070205.

Lopez-Sanchez, J.M., Cloude, S.R., and Ballester-Berman, J.D. 2012. “Rice phenology monitoring by means of SAR Polarimetry at X-Band.” *IEEE Transactions on Geoscience and Remote Sensing*, Vol. 50(No. 7): pp. 2695-2709. doi:10.1109/TGRS.2011.2176740.

Lopez-Sanchez, J.M., Vicente-Guijalba, F., Ballester-Berman, J.D., and Cloude, S.R. 2014. “Polarimetric response of rice fields at C-band: analysis and phenology retrieval.” *IEEE Transactions on Geoscience and Remote Sensing*, Vol. 52(No. 5): pp. 2977-2993. doi:10.1109/TGRS.2013.2268319.

Lopez-Sanchez, J.M., Vicente-Guijalba, F., Ballester-Berman, J.D., Cloude, S.R. 2015. “Influence of incidence angle on the coherent copolar polarimetric response of rice at X-Band.” *IEEE Geoscience and Remote Sensing Letters*, Vol. 12(No. 2): pp. 249-253. doi:10.1109/LGRS.2014.2334371.

Lopez-Sanchez, J.M., Vicente-Guijalba, F., Ballester-Berman, J.D., and Cloude, S.R. 2013. “Estimating phenology of agricultural crops from space.” In Proceedings of ESA Living Planet Symposium. Vol. ESA. Edinburgh, UK.

Maity, S., Patnaik, C., Chakraborty, M., and Panigrahy, S. 2004. “Analysis of temporal backscattering of cotton crops using a semiempirical model.” *IEEE Transactions on Geoscience and Remote Sensing*, Vol. 42(No. 3): pp. 577-587. doi:10.1109/TGRS.2003.821888.

Mattia, F., Le Toan, T., Picard, G., Posa, F.I., D’Alessio, A., Notarnicola, C., Gatti, A.M., Rinaldi, M., Satalino, G., and Pasquariello, G. 2003. “Multitemporal C-band

radar measurements on wheat fields." *IEEE Transactions on Geoscience and Remote Sensing*, Vol. 41(No. 7): pp. 1551-1560. doi:10.1109/TGRS.2003.813531.

McNairn, H., and Brisco, B. 2004. "The application of C-band polarimetric SAR for agriculture: a review." *Canadian Journal of Remote Sensing*, Vol. 30(No. 3): pp. 525-542. doi:10.5589/m03-069.

Moran, M.S., Alonso, L., Moreno, J.F., Cendrero Mateo, M.P., de la Cruz, D.F., and Montoro, A. 2012. "A RADARSAT-2 quad-polarized time series for monitoring crop and soil conditions in Barrax, Spain." *IEEE Transactions on Geoscience and Remote Sensing*, Vol. 50(No. 4): pp. 1057-1070. doi:10.1109/TGRS.2011.2166080.

Sánchez, N., Martínez-Fernández, J., González-Piqueras, J., González-Dugo, M.P., Baroncini-Turrichia, G., Torres, E., Calera, A., and Pérez-Gutiérrez, C. 2012b. "Water balance at plot scale for soil moisture estimation using vegetation parameters." *Agricultural and Forest Meteorology*, Vol. 166-167: pp. 1–9. doi:10.1016/j.agrformet.2012.07.005.

Sánchez, N., Martínez-Fernández, J., Calera, A., Torres, E., and Pérez-Gutiérrez, C. 2010. "Combining remote sensing and *in situ* soil moisture data for the application and validation of a distributed water balance model (HIDROMORE)." *Agricultural Water Management*, Vol. 98(No. 1): pp. 69-78. doi:10.1016/j.agwat.2010.07.014.

Sánchez, N., Martínez-Fernández, J., Scaini, A., and Pérez-Gutiérrez, C. 2012a. "Validation of the SMOS L2 soil moisture data in the REMEDHUS network (Spain)." *IEEE Transactions on Geoscience and Remote Sensing*, Vol. 50(No. 5): pp. 1602-1611. doi:10.1109/TGRS.2012.2186971.

Satalino, G., Mattia, F., Le Toan, T., and Rinaldi, M. 2009. “Wheat crop mapping by using ASAR AP data.” *IEEE Transactions on Geoscience and Remote Sensing*, Vol. 47(No. 2): pp. 527-30. doi:10.1109/TGRS.2008.2008026.

Skriver, H., Svendsen, M.T., and Thomsen, A.G. 1999. “Multitemporal C- and L-band polarimetric signatures of crops.” *IEEE Transactions on Geoscience and Remote Sensing*, Vol. 37(No. 5): pp. 2413–2429. doi:10.1109/36.789639.

Smith, A.M., and Buckley, J.R. 2011. “Investigating RADARSAT-2 as a tool for monitoring grassland in western Canada.” *Canadian Journal of Remote Sensing*, Vol. 37(No. 1): pp. 93-102. doi:10.5589/m11-027.

Steele-Dunne, S.C., McNairn, H., Monsivais-Huertero, A., Judge, J., Liu, P.W., and Papathanassiou, K. 2017. “Radar remote sensing of agricultural canopies: a review.” *IEEE Journal of Selected Topics in Applied Earth Observations and Remote Sensing*, Vol. 10(No. 5): pp. 2249-2273. doi:10.1109/JSTARS.2016.2639043.

Thompson, A.A. 2015. “Overview of the RADARSAT constellation mission.” *Canadian Journal of Remote Sensing*, Vol. 41(No. 5): pp. 401-407. doi:10.1080/07038992.2015.1104633.

Ulaby, F.T., Allen, C.T., Eger, G., and Kanemasu, E. 1984. “Relating the microwave backscattering coefficient to leaf area index.” *Remote Sensing of Environment*, Vol. 14(No. 1-3): pp. 113-133. doi:10.1016/0034-4257(84)90010-5.

Wiseman, G., McNairn, H., Homayouni, S., and Shang, J. 2014. “RADARSAT-2 polarimetric SAR response to crop biomass for agricultural production monitoring.” *IEEE Journal of Selected Topics in Applied Earth Observations and Remote Sensing*, Vol. 7(No. 11): pp. 4461-4471. doi:10.1109/JSTARS.2014.2322311.